IEEE Access
Multidisciplinary | Rapid Review | Open Access Journal

Received March 22, 2021, accepted May 5, 2021, date of publication May 11, 2021, date of current version June 7, 2021.

Digital Object Identifier 10.1109/ACCESS.2021.3079381

INS Fine Alignment With Low-Cost Gyroscopes: Adaptive Filters for Different Measurement Types

ITZIK KLEIN[1], (Senior Member, IEEE), AND YAAKOV BAR-SHALOM[2], (Life Fellow, IEEE)
[1]Department of Marine Technologies, University of Haifa, Haifa 3498838, Israel
[2]Electrical and Computer Engineering Department, University of Connecticut, Storrs, CT 06269, USA

Corresponding author: Itzik Klein (kitzik@univ.haifa.ac.il)

ABSTRACT Inertial navigation system stationary fine alignment process is a critical step in reducing the initial errors of the attitude and sensor biases. While many studies had been made for tactical grade systems, less attention was given to low-cost sensors, which are a major player in today's inertial sensors market. To fill this gap, a measurement strategy combining different INS aiding types is proposed, analyzed and compared using numerical simulations and field experiments. Additionally, an analytical linear observability analysis is made to support the numerical comparisons. Further, five types of adaptive Kalman filters with the proposed measurement strategy are compared to find the appropriate one to improve the alignment performance. The proposed measurement strategy can be used in other applications of stationary conditions such as land vehicles, robots or shoe-mounted inertial navigation systems.

INDEX TERMS Extended Kalman filter, fine alignment, inertial sensors, zero velocity updates.

I. INTRODUCTION

Inertial Navigation Systems (INS) are commonly used in many types of platforms such as autonomous vehicles, quadrotors, ships, airplanes and more. The INS popularity stems from the fact that it provides a full navigation solution consisting of the platform position, velocity and attitude vectors [1], [2]. INS is a standalone system that uses its own sensors, namely accelerometers and gyroscopes, to provide the navigation state. Also, INS is capable of working in any environment (air, sea, undersea, indoor and etc) and it is available in many different grades starting with low-cost low performance to high-cost high performance systems.

INS is a dead-reckoning system meaning it requires an initial navigation state vector prior to its operation. The initial position and velocity vectors are provided by external sensors (such as the global navigation satellite system) or information (like zero velocity). The initial attitude can also be provided by external sensors (such as a higher grade INS) or by using the INS inertial sensors in a process known as analytic coarse alignment. There, when the platform is in stationary conditions, the accelerometers and gyroscopes outputs are compared to the expected values of the gravity and Earth turn rate vectors, to calculate the initial attitude vector.

The associate editor coordinating the review of this manuscript and approving it for publication was Seung-Hyun Kong.

Jiang [3] proposed an alternative alignment formulation for stationary INS with analytical error assessment of both approaches. Silve *et al.* [4] presented a comprehensive literature review and error analysis of coarse alignment formulations for stationary strapdown INS. Recently, an analytical evaluation of partial coarse alignment for a gyro-free stationary INS system was derived in [5].

Usually, the accuracy of the coarse alignment process is not satisfactory, in particular if pure inertial navigation is required, and therefore external sensors or information are used to obtain a more accurate attitude vector in a process known as fine alignment (FA). For example, the global positioning system position and velocity measurements are used for in flight alignment [6], while underwater, the Doppler velocity log velocity measurements are employed in the alignment process. [7], [8]

In stationary alignment conditions the platform has zero velocity. This information is used as external measurement in the navigation filter to improve the attitude accuracy [9], [10]. As a consequence, in addition to the attitude vector, some of the inertial sensors error terms can also be estimated during the process [11], [12].

Recently, closed-form analytic solutions to the error-state covariance of the FA process and semi-analytic solutions to the convergence time of the error-state covariance were derived [13]. With such closed-form solutions at hand, insight

can be gained into the parameters involved in the FA process in preliminary design process.

Another measurement update usually applied is zero angular velocity with a version for gyroscopes capable of measuring the earth turn rate [12], [14] and ones which are not capable [15]. A less common measurement in stationary conditions is zero acceleration, where an assumption of small roll and pitch angles is made [12], [16].

Recent papers combining several measurement types includes [17] which used zero velocity, angular velocity and acceleration measurements for a stationary FA process using a tactical grade INS but without including the sensor error terms in the state vector. Later, [18] employed zero angular rate aiding for a tactical grade INS mounted on a vehicle and proposed means to overcome the quasi-stationary conditions. In [19] FA during the erecting process on a stationary base is considered using position and velocity updates.

In this paper, the scenario of stationary INS FA using low-cost gyroscopes is considered. The goal is to explore and combine all available measurement possibilities appearing in the literature in a single paper and find the best combination of measurement for the FA process using analytical, numerical and experimental analysis. The contributions of the paper are as follows:

1) Derivation of a measurement strategy and comparison between all possible measurement types for stationary INS FA using low-cost gyroscopes.
2) Analytical observability analysis for all measurement types for a low-cost gyroscopes INS.
3) Application of roll and pitch measurements for reduced INS sensor set for land vehicle dynamics, to the FA process regardless of the platform as long as stationary conditions apply.
4) Comparison for two different approaches for zero acceleration measurement. One requires small roll and pitch angles regardless of the accelerometers grade while the other requires high accelerometer grade regardless of the actual roll and pitch angles.
5) Comparison between five adaptive Kalman filters, with all measurement types, on the FA filter performance.

In addition to the numerical simulation, a field experiment using a smartphone was conducted to support the analysis.

The rest of the paper is organized as follows: Section II describes the FA process and EKF. Section III presents four different types of adaptive filters in the Kalman framework. Section IV shows the strategy of the paper while Section V gives the analytical observability analysis. Section VI presents the results and Section VII gives the conclusions.

II. FINE ALIGNMENT

The Extended Kalman Filter (EKF), with error state implementation, is commonly used in the fusion process between INS and aiding sensors [1], [12]. The error states are usually expressed in the North-East-Down (NED) reference frame with a 12 error-state linear model. It is assumed that the sensors coordinate frame coincides with the body frame. Since low-cost gyroscope sensors are addressed, the earth turn rate cannot be measured and hence neglected. The error-state vector is

$$\delta\mathbf{x} = \begin{bmatrix} \boldsymbol{\delta v}^n & \boldsymbol{\varepsilon}^n & \boldsymbol{b}_a & \boldsymbol{b}_g \end{bmatrix}^T \in \mathbb{R}^{12} \tag{1}$$

where $\delta\boldsymbol{v}^n = \begin{bmatrix} \delta v^N & \delta v^E & \delta v^D \end{bmatrix}^T$ is the velocity error vector, and $\boldsymbol{\epsilon}^n = \begin{bmatrix} \epsilon^N & \epsilon^E & \epsilon^D \end{bmatrix}^T$ is the attitude error state vector. $\boldsymbol{b}_a = \begin{bmatrix} b_{a,x} & b_{a,y} & b_{a,z} \end{bmatrix}^T$ and $\boldsymbol{b}_g = \begin{bmatrix} b_{g,x} & b_{g,y} & b_{g,z} \end{bmatrix}^T$ are accelerometer and gyro biases represented by random constants process. The state-space model associated with the error state vector is [11]

$$\delta\dot{\mathbf{x}} = \mathbf{A}\delta\mathbf{x} + \mathbf{G}\mathbf{w} \tag{2}$$

where $\mathbf{A}$, the system matrix, is defined by

$$\mathbf{A} = \begin{bmatrix} \mathbf{0}_{3\times3} & -\left[\boldsymbol{f}^n\times\right] & \boldsymbol{T}_b^n & \mathbf{0}_{3\times3} \\ \mathbf{0}_{3\times3} & \mathbf{0}_{3\times3} & \mathbf{0}_{3\times3} & \boldsymbol{T}_b^n \\ \mathbf{0}_{3\times3} & \mathbf{0}_{3\times3} & \mathbf{0}_{3\times3} & \mathbf{0}_{3\times3} \\ \mathbf{0}_{3\times3} & \mathbf{0}_{3\times3} & \mathbf{0}_{3\times3} & \mathbf{0}_{3\times3} \end{bmatrix} \tag{3}$$

$\boldsymbol{T}_b^n$ is the transformation matrix between the body and navigation frames, the shaping matrix $\mathbf{G}$ is

$$\mathbf{G} = \begin{bmatrix} \boldsymbol{T}_b^n & \mathbf{0}_{3\times3} & \mathbf{0}_{3\times3} & \mathbf{0}_{3\times3} \\ \mathbf{0}_{3\times3} & \boldsymbol{T}_b^n & \mathbf{0}_{3\times3} & \mathbf{0}_{3\times3} \\ \mathbf{0}_{3\times3} & \mathbf{0}_{3\times3} & \boldsymbol{I}_{3\times3} & \mathbf{0}_{3\times3} \\ \mathbf{0}_{3\times3} & \mathbf{0}_{3\times3} & \mathbf{0}_{3\times3} & \boldsymbol{I}_{3\times3} \end{bmatrix} \tag{4}$$

$\mathbf{w}$ is the process noise and the skew-symmetric matrix $\left[\boldsymbol{f}^n\times\right]$ is

$$\left[\boldsymbol{f}^n\times\right] = \begin{bmatrix} 0 & -f_d & f_e \\ f_d & 0 & -f_n \\ -f_e & f_n & 0 \end{bmatrix} \tag{5}$$

A. EXTENDED KALMAN FILTER

The EKF error-state closed loop implementation algorithm using the Joseph form for covariance update [12], [20] is implemented for the FA process using

$$\delta\hat{\mathbf{x}}_k^- = \mathbf{0} \tag{6}$$

$$\mathbf{P}_k^- = \Phi_{k-1}\mathbf{P}_{k-1}^+\Phi_{k-1}^T + \mathbf{Q}_{k-1} \tag{7}$$

$$\delta\hat{\mathbf{x}}_k^+ = \mathbf{K}_k\delta\mathbf{z}_k \tag{8}$$

$$\mathbf{K}_k = \mathbf{P}_k^-\mathbf{H}_k^T[\mathbf{H}_k\mathbf{P}_k^-\mathbf{H}_k^T + \mathbf{R}_k]^{-1} \tag{9}$$

$$\mathbf{P}_k^+ = [\mathbf{I} - \mathbf{K}_k\mathbf{H}_k]\mathbf{P}_k^-[\mathbf{I} - \mathbf{K}_k\mathbf{H}_k]^T + \mathbf{K}_k\mathbf{R}_k\mathbf{K}_k^T \tag{10}$$

where k is the time step index, $\delta\mathbf{x}_k^-$ is the a priori estimate of the error-state, $\delta\mathbf{x}_k^+$ is the a posteriori estimate of the error-state, $\delta\mathbf{z}_k$ is the measurement residual vector, $\mathbf{P}_k^-$ is the covariance of the a priori estimation error, $\mathbf{P}_k^+$ is the covariance of the posteriori estimation error, $\mathbf{K}_k$ is the Kalman gain, $\mathbf{Q}_k$ is the process noise covariance assumed to be constant for all samples, $\mathbf{R}_k$ is the measurement noise covariance assumed to be constant for all samples, Φ_k is the state transition matrix and $\mathbf{H}_k$ is the measurement matrix. The measurement residual vector and matrix are determined by the aiding types as addressed in the following subsection.

B. MEASUREMENT MODELS

1) ZERO VELOCITY UPDATE (ZV)

In stationary conditions the linear velocity is zero. This information, of zero velocity (ZV), is used to update the filter. Thus, the measurement residual (difference between INS measurement to its aiding counterpart) is [9], [10]

$$\delta\mathbf{z}_{\mathrm{ZV}} = \mathbf{v}^n_{\mathrm{INS}} - \mathbf{0}_{3\times1} = \mathbf{H}_{\mathrm{ZV}}\delta\mathbf{x} + \mathbf{v}_{\mathrm{ZV}} \tag{11}$$

where $\mathbf{v}^n_{\mathrm{INS}}$ is the calculated INS velocity vector, $\delta\mathbf{z}_{\mathrm{ZV}}$ is the measurement residual vector, $\mathbf{v}_{\mathrm{ZV}}$ is a zero mean white Gaussian measurement noise and the measurement matrix $\mathbf{H}_{\mathrm{ZV}}$ is

$$\mathbf{H}_{\mathrm{ZV}} = \begin{bmatrix} \mathbf{I}_{3\times3} & \mathbf{0}_{3\times3} & \mathbf{0}_{3\times3} & \mathbf{0}_{3\times3} \end{bmatrix} \tag{12}$$

2) ZERO ANGULAR RATE UPDATE (ZAR)

While in stationary conditions, the angular rate vector between the body and navigation frames is zero

$$\boldsymbol{\omega}_{nb} = \mathbf{0} \tag{13}$$

The corresponding measurement is

$$\tilde{\boldsymbol{\omega}}_{nb} = \boldsymbol{\omega}_{ib} - \boldsymbol{\omega}_{in} = \boldsymbol{b}_g \tag{14}$$

where $\boldsymbol{\omega}_{ib}$ is the angular velocity as measured by the gyroscopes and the transport rate $\boldsymbol{\omega}_{in}$ is neglected (stationary conditions and low-cost gyroscopes). Since stationary, the expected gyros output is only their biases as shown in (14). Thus, the measurement residual equation for zero angular rate (ZAR) updates during the FA process is [15]

$$\delta\mathbf{z}_{\mathrm{ZAR}} = \boldsymbol{b}_g - \mathbf{0}_{3\times1} = \mathbf{H}_{\mathrm{ZAR}}\delta\mathbf{x} + \mathbf{v}_{\mathrm{ZAR}} \tag{15}$$

where $\delta\mathbf{z}_{\mathrm{ZAR}}$ is the measurement residual vector, $\mathbf{v}_{\mathrm{ZAR}}$ is zero mean, random white Gaussian measurement noise, and the measurement matrix $\mathbf{H}_{\mathrm{ZAR}}$ is

$$\mathbf{H}_{\mathrm{zar}} = \begin{bmatrix} \mathbf{0}_{3\times3} & \mathbf{0}_{3\times3} & \mathbf{0}_{3\times3} & \mathbf{I}_{3\times3} \end{bmatrix} \tag{16}$$

3) ACCELEROMETER ROLL AND PITCH UPDATE (ARP)

Since the system is at stationary conditions the accelerometers output only the gravity vector. This property is utilized in the coarse alignment phase to directly estimate the initial roll and pitch angles before the FA process is applied. Another approach to calculate the roll and pitch angles, in stationary conditions, with a reduced set of accelerometers was suggested by [21] based on the works of [22] and [23] for land vehicle navigation. There, the two angles are calculated by

$$\phi = \sin^{-1}\left(-f_y/\sqrt{g^2 - f_x^2}\right) \tag{17}$$

$$\theta = \sin^{-1}\left(f_x/g\right) \tag{18}$$

where ϕ is the roll angle, θ is the pitch angle, g is the gravitational constant, f_x and f_y are the specific force components expressed in the body frame. Notice, that (17)-(18) are only valid for small pitch and roll angles, which is a reasonable assumption in land vehicles. Yet, for the general fine alignment setup the following equations should be used:

$$\phi = arctan2(-f_y, -f_z) \tag{19}$$

$$\theta = arctan2(f_x, \sqrt{f_y^2 + f_z^2}) \tag{20}$$

Taking the accelerometer measured roll and pitch (ARP) angles (19)-(20) as update and comparing to their estimated counterparts gives the measurement residual

$$\delta\mathbf{z}_{\mathrm{ARP}} = \begin{bmatrix} \phi_{\mathrm{INS}} - \phi \\ \theta_{\mathrm{INS}} - \theta \end{bmatrix} = \mathbf{H}_{\mathrm{ARP}}\delta\mathbf{x} + \mathbf{v}_{\mathrm{ARP}} \tag{21}$$

where $\delta\mathbf{z}_{\mathrm{ARP}}$ is the measurement residual vector, $\mathbf{v}_{\mathrm{ARP}}$ is a zero mean white Gaussian measurement noise, and $\mathbf{H}_{\mathrm{ARP}}$ is the measurement matrix. Notice, since small angles are addressed, the misalignment errors are equal to the Euler angles errors and therefore, the latter relates directly to the error state (1) by the following measurement matrix:

$$\mathbf{H}_{\mathrm{ARP}} = \begin{bmatrix} \mathbf{0}_{2\times3} & \mathbf{I}_{2\times2} & \mathbf{0}_{2\times4} & \mathbf{0}_{2\times3} \end{bmatrix} \tag{22}$$

Notice, that in situations when the small angles assumption does not hold, the following measurement matrix should be used:

$$\mathbf{H}_{\mathrm{ARP}} = \begin{bmatrix} \mathbf{0}_{2\times3} & \mathbf{H}_\theta & \mathbf{0}_{2\times4} & \mathbf{0}_{2\times3} \end{bmatrix} \tag{23}$$

where

$$\mathbf{H}_\theta = \begin{bmatrix} \frac{\cos\psi}{\cos\theta} & \frac{\sin\psi}{\cos\theta} \\ -\sin\psi & \cos\psi \end{bmatrix} \tag{24}$$

4) ZERO ACCELERATION UPDATE (ZA)

Another approach to take advantage of the fact that in stationary conditions the accelerometers measure the gravity vector is termed zero acceleration (ZA) update. There the specific force measurement is used directly instead of using it to calculate the roll and pitch angles. Although the same information is used, it is delivered in a different way to the filter and thus, due to the nonlinear system, may lead to a different filter performance.

The specific force vector expressed in the navigation frame is related to the one expressed in the body frame by

$$\mathbf{f}^n = \mathbf{T}^n_b\mathbf{f}^b \tag{25}$$

The difference between the measured and actual specific force is

$$\delta\mathbf{f}^n = \mathbf{f}^n_{\mathrm{INS}} - \mathbf{f}^n = \mathbf{T}^n_{b,\mathrm{INS}}\mathbf{f}^b_{\mathrm{INS}} - \mathbf{f}^n \tag{26}$$

Perturbation around the nominal trajectory and removing second order error terms, yields the measurement residual

$$\delta\mathbf{z}_{\mathrm{ZA1}} = -(\boldsymbol{f}^n\times)\boldsymbol{\epsilon}^n + \mathbf{T}^n_b\boldsymbol{b}_g = \mathbf{H}_{\mathrm{ZA1}}\delta\mathbf{x} + \mathbf{v}_{\mathrm{ZA1}} \tag{27}$$

where $\delta\mathbf{z}_{\mathrm{ZA1}}$ is the measurement residual vector, $\mathbf{v}_{\mathrm{ZA1}}$ is a zero mean white Gaussian measurement noise and the measurement matrix $\mathbf{H}_{\mathrm{ZA1}}$ is given by (`ZA1` implementation)

$$\mathbf{H}_{\mathrm{ZA1}} = \begin{bmatrix} \mathbf{0}_{3\times3} & -(\boldsymbol{f}^n\times) & \mathbf{T}^n_b & \mathbf{0}_{3\times3} \end{bmatrix} \tag{28}$$

Another approach to formulate the ZA measurement is described in [12]. There, small roll and pitch angles are considered. In such a case, the term $-(\boldsymbol{f}^n\times)\boldsymbol{\epsilon}^n$ can be replaced with the known local gravity vector expressed in the navigation frame, $\boldsymbol{g}^n$ and a noise term to represent the navigation frame disturbances (due to the small roll and pitch angle). In this implementation (ZA2), the measurement residual and matrix are

$$\delta\mathbf{z}_{\mathrm{ZA}} = (\boldsymbol{g}^n\times)\boldsymbol{\epsilon}^n + \mathbf{T}_b^n\boldsymbol{b}_g + \boldsymbol{f}_d = \mathbf{H}_{\mathrm{ZA}}\delta\mathbf{x} + \mathbf{v}_{\mathrm{ZA}} \quad (29)$$

$$\mathbf{H}_{\mathrm{ZA}} = \begin{bmatrix}\mathbf{0}_{3\times3} & (\boldsymbol{g}^n\times) & \mathbf{T}_b^n & \mathbf{0}_{3\times3}\end{bmatrix} \quad (30)$$

where $\boldsymbol{f}_d$ represents the navigation frame disturbances and

$$\boldsymbol{g}^n = \begin{bmatrix}0 & 0 & g\end{bmatrix}^T \quad (31)$$

III. ADAPTIVE KALMAN FILTERS

The motivation of using adaptive approaches within the Kalman filter algorithms, is to examine the possibility they will improve the filter performance in terms of accuracy and time to converge. In particular, in situations where the process or measurement noise covariance are not exactly known.

A. EXPONENTIAL DATA WEIGHTING (EKF-E)

Generally, there are two methods for preventing divergence: fictitious process noise injection and exponential data weighting. Both methods work by preventing the predicted error covariance P_k^+, and hence the Kalman gain K_k from going to zero with k. This means that as time k increases, the process and measurement noise covariances decrease, so that we are giving more credibility to the recent data by decreasing the noise covariance exponentially [24]. The model covariance matrices are set to [24], [25]

$$\mathbf{R}_k = \mathbf{R}\alpha^{-2(k+1)} \quad (32)$$

$$\mathbf{Q}_k = \mathbf{Q}\alpha^{-2(k+1)} \quad (33)$$

for some $\alpha \geq 1$ and constant matrices $\mathbf{R}$ and $\mathbf{Q}$.

B. SCALING FACTOR ON THE PROCESS NOISE COVARIANCE (EKF-Q)

As shown in [26] increasing the process noise will lead to an improvement in the convergence rate of the filter. As pointed out in [27], since this additive positive definite matrix is selected arbitrarily, it can be combined into a scaling factor on the process noise covariance, such that (7) is modified as

$$\mathbf{P}_k^- = \Phi_{k-1}\mathbf{P}_{k-1}^+\Phi_{k-1}^T + \alpha_Q\mathbf{Q}_{k-1} \quad (34)$$

where α_Q is a scaling factor greater than one.

C. SCALING FACTOR ON THE MEASUREMENT NOISE COVARIANCE (EKF-R)

This method aims to improve the convergence rate of the filter considering the opposite of the ''underweighting'' approach [27]. The purpose of ''underweighting'' is to prevent the state error covariance from converging too quickly from very precise measurements. This process effectively slows the convergence of the filter; however it contains some desirable robustness to erroneous measurements. To create the opposite behavior, the gain (9) and covariance update (10) equations are modified using a scaling factor

$$\mathbf{K}_k = \mathbf{P}_k^-\mathbf{H}_k^T[\mathbf{H}_k\mathbf{P}_k^-\mathbf{H}_k^T + \frac{1}{\alpha_R}\mathbf{R}_k]^{-1} \quad (35)$$

$$\mathbf{P}_k^+ = [\mathbf{I} - \mathbf{K}_k\mathbf{H}_k]\mathbf{P}_k^-[\mathbf{I} - \mathbf{K}_k\mathbf{H}_k]^T + \frac{1}{\alpha_R}\mathbf{K}_k\mathbf{R}_k\mathbf{K}_k^T \quad (36)$$

where α_R is a scaling factor greater than one.

D. SCALING FACTOR ON THE ERROR STATE COVARIANCE (EKF-P)

Another implementation of exponential data weighting was suggested in [28]. There, a scale factor was used to improve the stability the system, at the cost of performance. However, since this scaling factor increases the covariance it may lead to faster convergence. To employ, this approach (7) is modified as

$$\mathbf{P}_k^- = \alpha_P\Phi_{k-1}\mathbf{P}_{k-1}^+\Phi_{k-1}^T + \mathbf{Q}_{k-1} \quad (37)$$

where α_P is a scaling factor greater than one.

IV. STRATEGY

Four different measurement types, namely: ZV, ZAR, ARP and ZA, where the latter has two approaches for implementation in the filter. Before, describing our proposed strategy we elaborate on the difference between the two. Notice, in the measurement equation (26) knowledge of $\boldsymbol{f}^n$ is required. For stationary conditions, the specific force vector is given by

$$\boldsymbol{f}^b = \begin{bmatrix}\sin\theta \\ -\cos\theta\sin\phi \\ -\cos\theta\cos\phi\end{bmatrix} g \quad (38)$$

In the first ZA implementation, (27), the roll and pitch angles are taken from the calculated INS solution where in the initial step they are determined by the coarse alignment process. Thus, as the accelerometer quality increases (reduced level of error terms) the initial roll and pitch accuracy increases resulting in a better filter performance since (38) is satisfied. However, for low-cost accelerometers a higher error in (38) is expected, leading to a degradation of the filter performance. On the other hand, the second ZA implementation uses the gravity vector (31) instead of (38) in the measurement (29). Thus, it does not depend on the accelerometer quality. Rather, it requires that the actual roll and pitch angles during the alignment will be small so that (38) will give $\boldsymbol{f}^n \approx -\boldsymbol{g}^n$. The answer which one of the ZA implementations is suitable, depends on the actual roll and pitch angles, gyroscopes and accelerometer quality and needs to be numerically evaluated. Therefore, our first step will be a numerical comparison between the two.

Regardless of the initial roll and pitch angles or accelerometer grade, the ZV and ZAR measurement models will yield the same filter behaviour. The ARP update depends on the gyroscope and accelerometer quality. The ARP measurement

residual (22) depends on the calculated accelerometer roll and pitch angles and also on the INS calculated ones which in turn depend on the gyroscopes' outputs. Therefore, for low-cost sensors with high error terms in the sensor measurements, this update is questionable. However, using ZAR update, the gyros' bias are measured directly by (15), thus it is expected that the accuracy of the INS roll and pitch will increase. Therefore, it is likely that, ARP update should be combined with ZAR update. This assumption of improved accuracy is made since by using the gyros measured angular velocity vector, the transformation matrix between body to navigation frame is updated and then the updated Euler angles can be extracted. Thus, if the gyro measurements had no bias it is likely that the Euler angles will be more accurate.

Based on the discussion above we examine the following set of measurements models with the FA process.

1) **ZV**: Zero velocity update using the measurement residual (11) and matrix (12). This is the most commonly used measurement type in the literature and represents the minimum set of measurements.
2) **ZVZAR**: Zero velocity and zero angular rate updates. Those two updates do not depend on the initial roll and pitch angles. The resulting measurement matrix from the combination of (12) and (16) is

$$\mathbf{H}_{\texttt{ZVZAR}} = \begin{bmatrix} \mathbf{I}_{3\times3} & \mathbf{0}_{3\times3} & \mathbf{0}_{3\times3} & \mathbf{0}_{3\times3} \\ \mathbf{0}_{3\times3} & \mathbf{0}_{3\times3} & \mathbf{0}_{3\times3} & \mathbf{I}_{3\times3} \end{bmatrix} \tag{39}$$

3) **ZVZARARP**: Zero velocity, zero angular rate and accelerometer based roll and pitch updates. This model enhances the previous one with a direct measurement of the roll and pitch angles.

$$\mathbf{H}_{\texttt{ZVZARARP}} = \begin{bmatrix} \mathbf{I}_{3\times3} & \mathbf{0}_{3\times3} & \mathbf{0}_{3\times3} & \mathbf{0}_{3\times3} \\ \mathbf{0}_{2\times2} & \mathbf{I}_{2\times3} & \mathbf{0}_{2\times4} & \mathbf{0}_{2\times3} \\ \mathbf{0}_{3\times3} & \mathbf{0}_{3\times3} & \mathbf{0}_{3\times3} & \mathbf{I}_{3\times3} \end{bmatrix} \tag{40}$$

4) **ZVZARZA**: Zero velocity, zero angular rate and zero acceleration updates. Here, ARP is replaced by the ZA measurement model.

$$\mathbf{H}_{\texttt{ZVZARZA}} = \begin{bmatrix} \mathbf{I}_{3\times3} & \mathbf{0}_{3\times3} & \mathbf{0}_{3\times3} & \mathbf{0}_{3\times3} \\ \mathbf{0}_{3\times3} & (\boldsymbol{g}^n\times) & \mathbf{T}_b^n & \mathbf{0}_{3\times3} \\ \mathbf{0}_{3\times3} & \mathbf{0}_{3\times3} & \mathbf{0}_{3\times3} & \mathbf{I}_{3\times3} \end{bmatrix} \tag{41}$$

After the measurement types have been selected, their contribution in estimating the error state (1) is evaluated using observability analysis. To that end, analytical linear observability analysis, as detailed in the following section, is performed. After the analytical observability analysis, we examine the four types of measurement sequences on the regular EKF filter and only then on the other adaptive filters as presented in Section III.

V. OBSERVABILITY ANALYSIS

In the FA process the system is held in stationary conditions and without loss of generality we assume the body and navigation coordinate frames coincide, thus $\boldsymbol{T}_b^n = \boldsymbol{I}_3$. This assumption is made to ease the mathematical derivation and enable to gain insight from the observability analysis. To derive analytically the observable subspace, we follow the analytical observability approach as in [9], [29] and start by calculating the observability matrix.

The observability matrix at $t = 0$ is constructed to examine the rank of the observability error-states. Notice, that at $t = 0$ the system (2) is linear and thus the observability matrix is a valid test. The observability matrix is defined by the system matrix and measurement matrix as

$$\mathcal{O} = \begin{bmatrix} \mathbf{H} \\ \mathbf{HA} \\ \vdots \\ \mathbf{HA}^{m-1} \end{bmatrix} \tag{42}$$

where m is the error state dimension which is 12 in our case. Further, the observable and unobservable subspaces are spanned by the observability matrix image $Im(\mathcal{O})$ and kernel $ker(\mathcal{O})$, where the state space can be spanned using $Im(\mathcal{O}) \oplus ker(\mathcal{O})$. A state transformation matrix is constructed by taking n (the rank of $\mathcal{O}$) independent rows from $Im(\mathcal{O})$ and constructing $\mathcal{O}_1$. The other $12 - n$ independent vectors, orthogonal to $\mathcal{O}_1$, are found by the null space of $\mathcal{O}_1$ to construct $\mathcal{O}_2$, that is $ker(\mathcal{O})$. In that manner, a state transformation matrix, $\mathbf{T}$, from the original state vector (1) to the observable and unobservable states is formed

$$\mathbf{T} = \begin{bmatrix} \mathcal{O}_1 \\ \mathcal{O}_2 \end{bmatrix} \tag{43}$$

1) ZERO VELOCITY UPDATE

Plugging the system (3) and measurement (12) matrices into the observability matrix yields a rank of eight, meaning that there are only eight observable states or a linear combination of them. Next, the state transformation matrix (43) is formed to give the observable subspace (OS):

$$\texttt{OS}_{\mathbf{ZV}} = \begin{bmatrix} v_n \\ v_e \\ v_d \\ \epsilon_N - b_{a,y}/g \\ \epsilon_E + b_{a,x}/g \\ b_{a,z} \\ b_{g,x} \\ b_{g,y} \end{bmatrix} \in \mathbb{R}^8 \tag{44}$$

Notice that $\texttt{OS}_{\mathbf{ZV}}$ contains linear combinations of the horizontal biases and misalignment errors.

2) ZERO VELOCITY AND ZERO ANGULAR RATE UPDATE

In the same manner, the observability matrix using the linear and angular velocity update measurement matrix (12) and (16) was found to have rank of nine. There, the addition of the zero angular velocity vector measurement increased the system by only one more observable state. The resulting

observable subspace is

$$\mathrm{OS}_{\mathbf{ZVZAR}} = \begin{bmatrix} v_n \\ v_e \\ v_d \\ \epsilon_N - b_{a,y}/g \\ \epsilon_E + b_{a,x}/g \\ b_{a,z} \\ b_{g,x} \\ b_{g,y} \\ b_{g,z} \end{bmatrix} \in \mathbb{R}^9 \tag{45}$$

Comparing (45) to (44) we observe that the addition of the zero angular velocity measurement added the gyro's z-axis bias, $b_{g,z}$ to the OS.

3) ZERO VELOCITY, ZERO ANGULAR RATE AND ZERO ACCELERATION UPDATE

The measurement matrix is constructed using the ZV measurement matrix (12), the ZAR measurement matrix (16) and the ZA measurement matrix (30). Using (42), the resulting number of observable states is 11, where the OS is

$$\mathrm{OS}_{\mathbf{ZVZARZA}} = \begin{bmatrix} v_n \\ v_e \\ v_d \\ \epsilon_N \\ \epsilon_E \\ b_{a,x} \\ b_{a,y} \\ b_{a,z} \\ b_{g,x} \\ b_{g,y} \\ b_{g,z} \end{bmatrix} \in \mathbb{R}^{11} \tag{46}$$

Comparing (45) to (46) we observe that the addition of ZA update managed to remove the linear dependence of the misalignment angle ϵ_N to $b_{a,y}$ and ϵ_E to the bias $b_{a,x}$ added all the four states to the OS. Also, the same observable space will result if instead of (30) the other ZA implementation, (28), is used.

4) ZERO VELOCITY, ZERO ANGULAR RATE AND ACCELEROMETER ROLL AND PITCH UPDATE

In this case, the measurement matrix is constructed using the ZV measurement matrix (12), the ZAR measurement matrix (16) and the ARP measurement matrix (22). Substituting the resulting measurement matrix in the observability matrix (42) the resulting rank is 11 and the OS is equal to the ZVZAEZA update

$$\mathrm{OS}_{\mathbf{ZVZARARP}} = \mathrm{OS}_{\mathbf{ZVZARZA}} \tag{47}$$

VI. ANALYSIS AND RESULTS

A stationary FA simulation was employed for the analysis using standard navigation equations. The true value of the velocity vector, roll, pitch and yaw angles were set to zero throughout the simulation. Their initial conditions were randomized in each run using a zero mean white Gaussian noise with standard deviation (STD) of 0.5m/s for the velocity vector, 3deg for the roll and pitch angles and 10deg for the yaw angle.

TABLE 1. Accelerometers and gyroscopes error terms specifications.

Error Term	Accelerometers	Gyroscopes
Bias	$30\mathrm{m}g$	30deg/hr
Random walk	$230\mu g/\sqrt{\mathrm{Hz}}$	$4 \times 10^{-3}(\mathrm{deg/s})/\sqrt{\mathrm{Hz}}$

The FA process was carried out for a time duration of 60s. The inertial sensors provide measurements with a sampling rate of 100Hz. The accelerometers and gyroscopes are modeled with a constant bias and a random walk process with parameters provided in Table 1. The EKF is employed using (6)-(10) with the error-state vector (1), system matrix (3) and shaping matrix (4). For the initial error state covariance, $\mathbf{P}_0$, the same initial conditions as described above for the velocity and Euler angles were used while for the accelerometer and gyroscopes the initial biases (Table 1) were multiplied by a factor of 3.

To evaluate the proposed approach, 50 Monte-Carlo (MC) runs were made, where for each run random initial conditions were used and in each time-step random values for the sensors outputs and measurement noise were drawn. Since stationary conditions are given and also the velocity estimation it is not the purpose of the FA process, we don't address the velocity estimation performance. Focus is given to the Euler angles and the inertial sensors error terms. For those states, we present the MC mean and STDs in the following figures.

A. COMPARISON BETWEEN ZA IMPLEMENTATIONS

As discussed in Section IV, first the two implementations of ZA measurement are compared. For the first implementation, ZA1, the measurement residual and matrix are given by (27) and (28) while for the second implementation, ZA2 (29) and (30) are used. For both implementations, the ZV and ZAR measurement models are added and the approaches are labeled as ZVZARZA1 and ZVZARZA2. The comparison is made using the regular EKF with two sets for accelerometer parameters: 1) as presented in Table 1 with 3deg STD for the initial roll and pitch angles denoted as case 1 and 2) 3mg accelerometer bias and 0.3deg for the initial roll and pitch angles denoted as case 2.

Since the ZA measurement model influences the observability and performance of the roll, pitch and accelerometer biases in the x and y axes, only their error-states are addressed in this section for the comparison.

As discussed in Section IV, ZA1 performance should increase as the accelerometer quality increases (lower level of bias and noise) thus, it is expected to work better in case 2. ZA2 model performance should improve for smaller roll and pitch angles. Since we consider zero nominal roll and pitch it is expected that ZA2 will also give better performance for case 2 since its initial roll and pitch angles are smaller by a factor of ten.

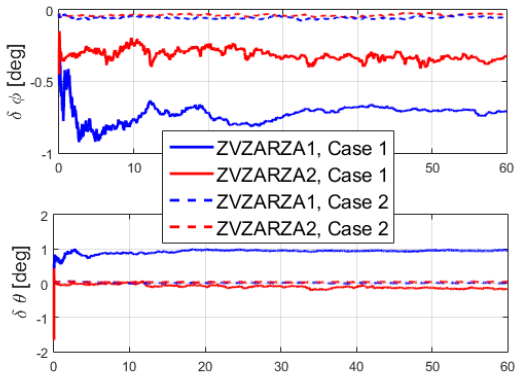

FIGURE 1. Monte Carlo mean error of the roll ($\delta\phi$) and pitch ($\delta\theta$) angles using the two implementations of the ZA measurement model.

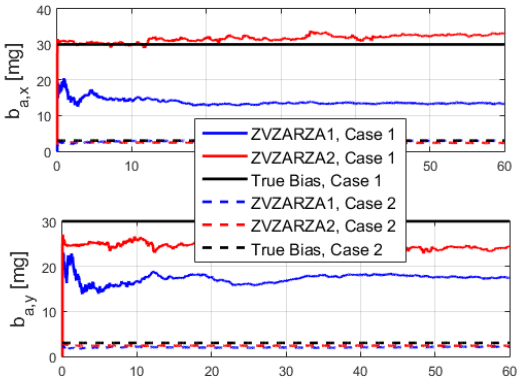

FIGURE 2. Monte Carlo mean error of the x and y accelerometer bias components using the two implementations of the ZA measurement model.

The mean MC results for the roll and pitch error are presented in Figure 1. The solid lines show the results of case 1 and in the dashed lines are for case 2. For ZVZARZA1 case 1, the mean error is 0.7 for the roll and 1deg for the pitch while for ZVZARZA2 the mean error is 0.3 and 0.15deg, respectively. The corresponding STDs for case 1 are 2deg for ZVZARZA1 and 1.3deg for ZVZARZA2. Thus, ZVZARZA2 model outperformed ZVZARZA1 for case 1. For case 2, both approaches obtained similar performance for the mean, yet ZVZARZA1 STD was two times bigger than ZVZARZA2 STD. Also, the convergence time is approximately five seconds for ZVZARZA1 and up to one secnod for ZVZARZA2.

The mean MC results for the accelerometer biases are presented in Figure 2. For case 1, ZVZARZA1 managed to estimate about 50% of the actual bias while ZVZARZA2 about 85% of it. The same level of accuracy was kept in case 2 for ZVZARZA2 and improved to about 65% for ZVZARZA1. The STDs were 30 and 20mg for ZVZARZA1 and ZVZARZA2, respectively for case 1 and 2 and 0.5mg for case 2. Based on the above results and since we are addressing low-cost sensors as presented in Table 1, ZA2 (29)-(30) is chosen for the measurement model implementation for the rest of the paper and will be addressed as ZA.

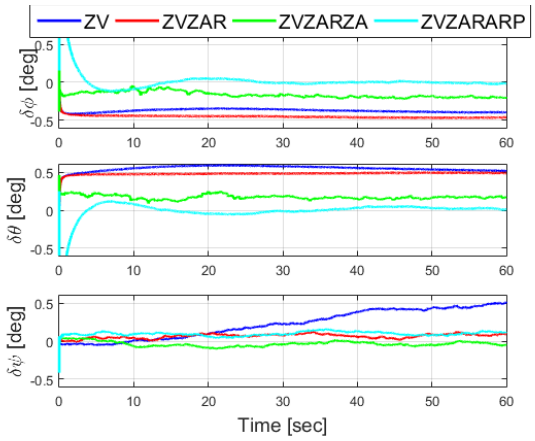

FIGURE 3. Monte Carlo mean error of the Euler angles using all four measurement models with a regular EKF.

B. EKF WITH DIFFERENT MEASUREMENT TYPES

The standard EKF filter with the four type of measurement models ZV, ZVZAR, ZVZARARP and ZVZARZA is addressed. The objective, is to determine the best measurement model for the FA process using low-cost sensors.

Figure 3 shows the results of the mean MC runs for the Euler angles. ZV and ZVAR obtained the almost the same performance for the roll and pitch angles with an error of 0.5deg. As expected, for ZV the yaw error diverges rapidly since it is not part of the observable subspace (44). Actually, the yaw angle is not observable for all the measurement models addressed. However, since ZAR helps to estimate the gyroscope biases, the divergence of the yaw error is decreased in all other measurement models.

Both ZVZAPARP and ZVZARZA observable subspace (47) shows that the roll and pitch angles become observable. Between the two, ZVZAPARP obtained a mean error less than 0.01deg for both pitch and roll. The corresponding STDs of the Euler angles are presented in Figure 4. As shown in the analytical observable subspaces (44)–(46) for all measurement models the yaw angle is not observable. This analytical derivation is supported by the diverging yaw error STDs of all measurement models. As for the roll and pitch STDs, ZV and ZVZAR produces the same value while ZVZARARP has the lowest STD of 0.08deg.

The accelerometer biases error states MC mean and STD are presented in Figures 5–6. The accelerometer z-axis bias is observable by the ZV measurements (44) which are present in all measurement models. Thus, the STD of all models converge at the same time to values less than 0.05mg except for ZVZARZA that converges to 0.9mg. On the other, the x and y biases are not directly observable by ZV measurements and therefore do not converge in the ZV and ZVZAR measurement models. For the ZVZARARP and ZVZARZA models, those biases are directly observable (46). Comparing the two, ZVZARARP results in a convergence of the biases STD and an accurate estimation of the biases, while for ZVZARZA the STD remains fixed with a value 20mg and a 85% estimation of the actual bias.

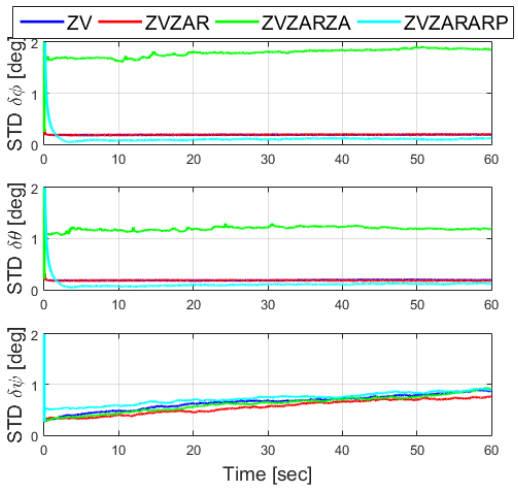

FIGURE 4. Monte Carlo standard deviation of the Euler angles using all four measurement models with a regular EKF.

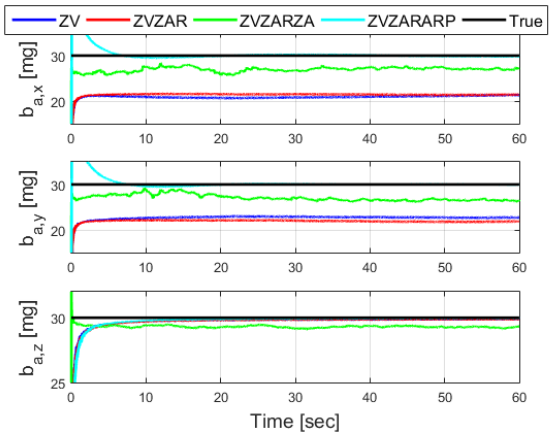

FIGURE 5. Monte Carlo mean error of the accelerometer biases using all four measurement models with a regular EKF.

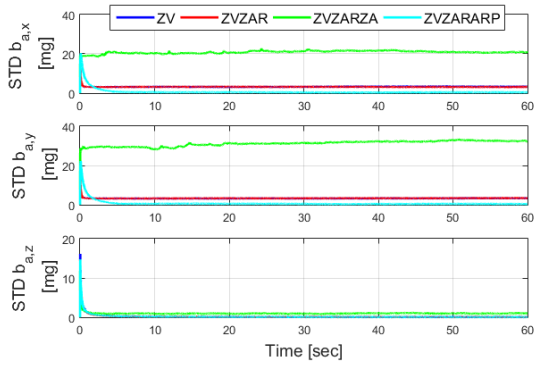

FIGURE 6. Monte Carlo standard deviation of the accelerometer biases using all four measurement models with a regular EKF.

The gyroscope biases error states MC mean and STD are presented in Figures 7–8. The ZAR measurement makes all three biases observable while ZV enables only the observability of x and y components. This is observed in the behavior of the STDs. The convergence of all measurement models, except ZV, is equal in the z direction and the bias is accurately

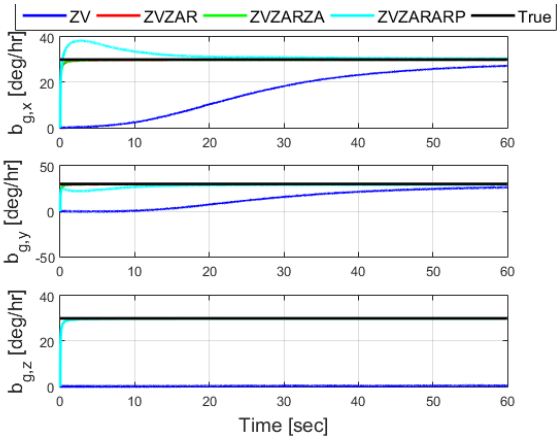

FIGURE 7. Monte Carlo mean error of the gyroscopes biases using all four measurement models with a regular EKF.

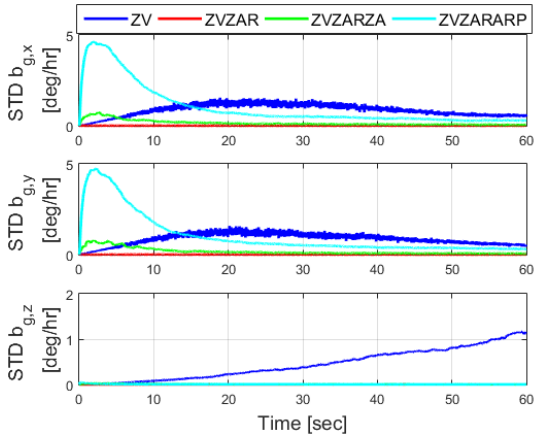

FIGURE 8. Monte Carlo standard deviation of the gyroscopes biases using all four measurement models with a regular EKF.

estimated. At the end of the trajectory, the x and y biases are estimated by all measurement models, however with different convergence rate. ZVZAR and ZVZARZA converge after two seconds, ZVZARARP after 16s and ZV after 60s.

Lastly, the OS of ZV (44) and ZVZAR (45) showed a linear combination of the misalignment errors and accelerometer biases are observable. This connection was removed in the OS of ZVZARARP and ZVZARZA models (46) enabling direct observability of those states. Figure 9 presents those linear connections for the four measurement models. For ZV and ZVZAR models, the results are almost the same since only ZV contributes to the estimation of those states. There, a convergence to a value of 0.6 is achieved. For the ZVZARZA, the convergence is to a value more than two times bigger. This is attributed to the relatively high STDs obtained for the Euler (Figure 4) and accelerometer bias (6) states. ZVZARARP obtained the best performance were the convergence value was reduced to 0.2.

C. ADAPTIVE FILTER COMPARISON

In the previous section, ZVZARARP was found to be the best measurement model for FA process using a regular EKF.

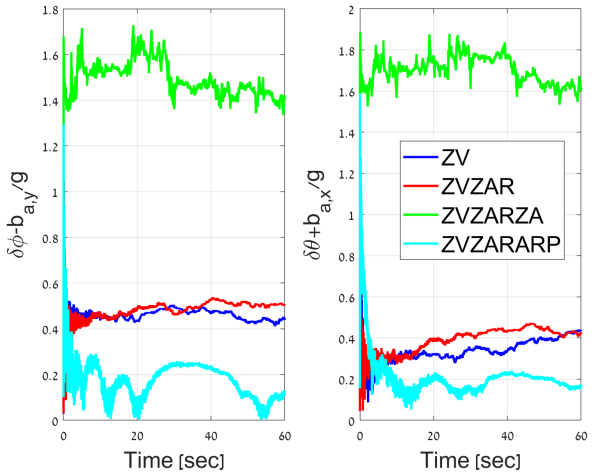

FIGURE 9. Monte Carlo standard deviation of the observable linear combinations using all four measurement models with a regular EKF.

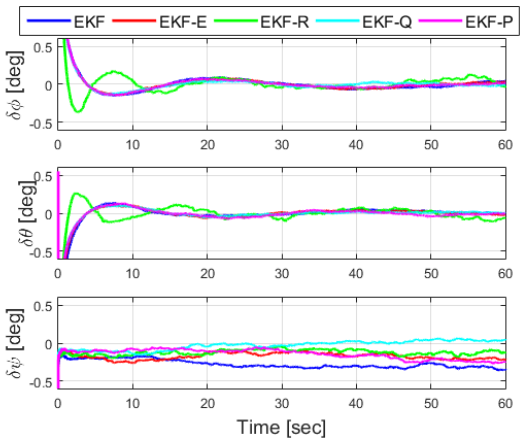

FIGURE 10. Monte Carlo mean error of the Euler angles using ZVZARARP measurement model with five different adaptive EKFs.

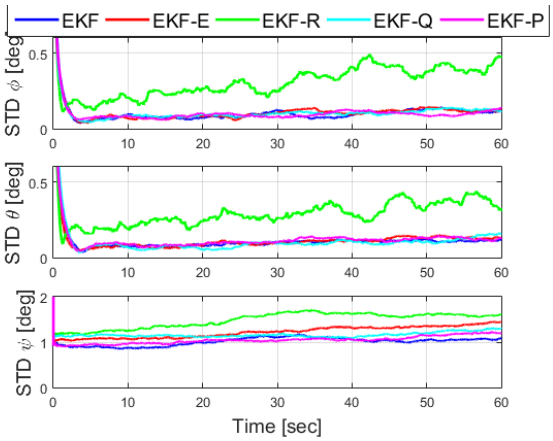

FIGURE 11. Monte Carlo standard deviation of the Euler angles using ZVZARARP measurement model with five different adaptive EKFs.

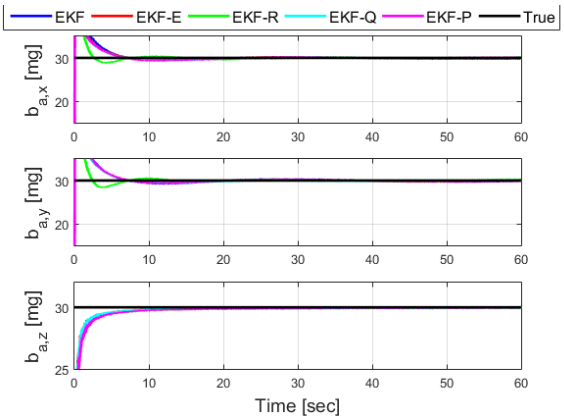

FIGURE 12. Monte Carlo mean error of the accelerometer biases using ZVZARARP measurement model with five different adaptive EKFs.

In this section, we examine ZVZARARP with the other four adaptive filters described in Section III, namely EKF-Q, EKF-R, EKF-P and EKF-E. For each type of filter many values for the scaling factors were examined. To produce the following figures, the scale factor that gave the best performance in each filter was used. For the EKF-E filter $\alpha = 1.0001$, for EKF-R $\alpha_R = 50$, for EKF-Q $\alpha_Q = 1.00005$ and for EKF-P $\alpha_P = 1.00001$.

The Euler angles error states MC mean and STD are presented in Figures 10–11. In the roll and pitch angles mean and STD no major difference was obtained between the filters except for EKF-R. There, the STD diverges and the error fluctuates with higher overshot, yet the mean error over time is equal between all filters. For the yaw error, the regular EKF divergence is the fastest one with en error of 0.3deg after 60s while EKF-Q has the lowest error of 0.04deg.

For the accelerometer biases error states, only the MC mean is presented in Figure 12 since the STDs are equal. For $b_{a,z}$ there is no difference between the filters. For $b_{a,x}$ and $b_{a,y}$ the convergence time of all filters are same although their behavior is a function of time is different. At the end of the scenario EKF-Q improves the regular EKF by 0.1mg.

The gyroscope bias error states MC mean and STD are presented in Figures 13-14. For the STDs, no difference was observed in $b_{g,z}$, however, for $b_{g,x}$ and $b_{g,y}$ EKF-R convergence time is 2.5 times faster than the other filters. As a consequence, the mean error has the same behavior. Also, the EKF-R error at the end of the scenario is lower by 0.5deg/hr than the regular EKF. For the $b_{g,z}$, the mean MC error of the EKF-R convergences after 0.4s while the other filters it takes approximately 2.5s.

D. FIELD EXPERIMENT

To support the simulation results, a field experiment was conducted using a Samsung Galaxy A7 smartphone. It is equipped with ST Microelectronics LSM6DSL inertial module. The accelerometer and gyroscopes readings were recorded at 100Hz while the smartphone was set stationary on a table with approximately zero roll and pitch angles. The recording duration was 70.4s. To estimate the actual bias experienced by the sensors, the average of the readings was calculated in each axis and the resulting value was treated as the zero offset bias (taking into account the gravity value).

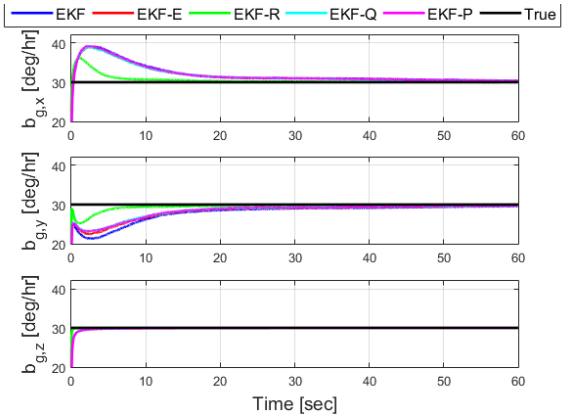

FIGURE 13. Monte Carlo mean error of the gyroscope biases using ZVZARARP measurement model with five different adaptive EKFs.

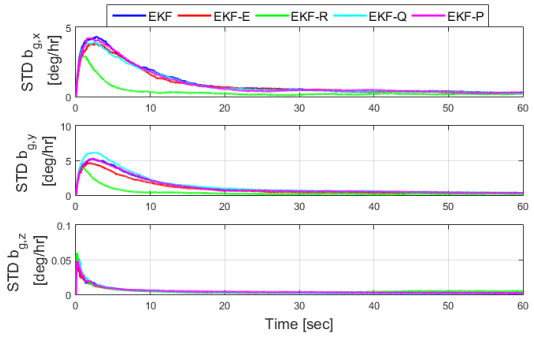

FIGURE 14. Monte Carlo standard deviation of the gyroscope biases using ZVZARARP measurement model with five different adaptive EKFs.

The standard EKF filter with the four type of measurement models ZV, ZVZAR, ZVZARARP and ZVZARZA was examined.

The Euler angles errors are presented in Figure 15. As observed in the simulation results, the ZV yaw error diverges rapidly since it is not part of the observable subspace (44). Actually, the yaw angle is not observable for all the measurement models addressed. However, since ZAR helps to estimate the gyroscope biases, the divergence of the yaw error is decreased in all other measurement models. ZVZAPARP obtained the best performance with roll and pitch mean error of 0.01deg while ZVZARZA obtined 0.015deg. The estimation of the accelerometer biases is shown in Figure 16 for the last 20 seconds of the experiment in order to visualize the difference between the measurement types. The z-axis accelerometer bias was estimated with all measurement types as expected from the observability analysis in Section V. As in the simulation results, ZVZARZA obtained the worst performance. For the x-axis accelerometer bias, ZVZARARP managed to estimate 89% of the bias while ZV and ZVZAR about 80%. In the same manner, ZVZARARP managed to estimated 81% of the y-axis accelerometer bias while ZV and ZVZAR about 83%.

Figure 17 presents the estimation of the gyroscopes biases. The ZAR measurement makes all three biases observable

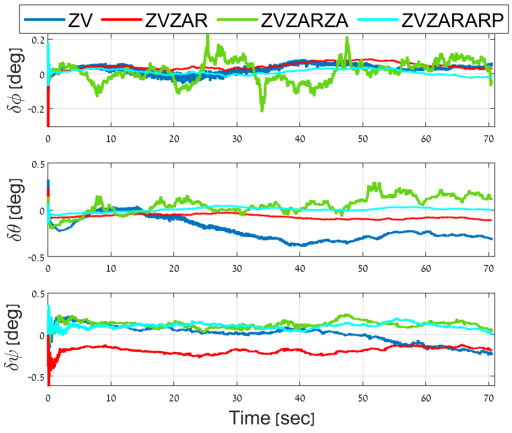

FIGURE 15. Euler angles error using all four measurement models with a regular EKF for the smartphone experiment.

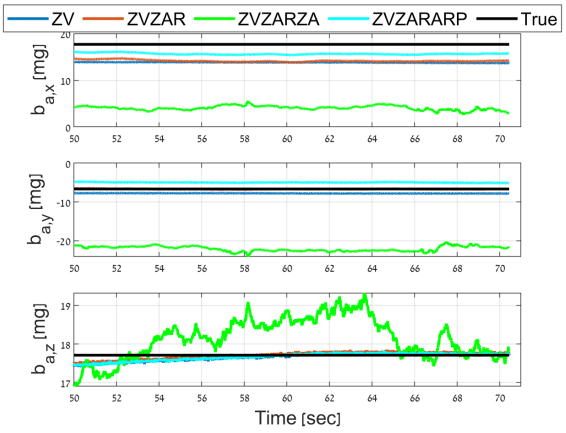

FIGURE 16. Accelerometer biases estimation using all four measurement models with a regular EKF for the smartphone experiment.

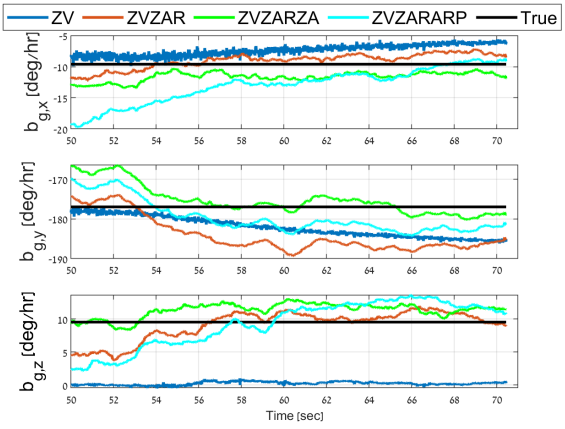

FIGURE 17. Gyroscope biases estimation using all four measurement models with a regular EKF for the smartphone experiment.

while ZV enables only the observability of x and y components. The performance of ZVZARZA and ZVZARARP was superior to that of ZVZAR.

The experiment was repeated two more times to validate the analysis and similar results were obtained.

VII. CONCLUSION

The stationary fine alignment process with low-cost gyroscopes was addressed. Four types of measurement models are available in such conditions: zero velocity, zero angular rate, accelerometer roll and pitch and zero acceleration, where for the latter two implementations were examined. After examining the benefits of those measurements, a strategy for combination between them was proposed. Four combinations of measurement models were suggested, namely: ZV, ZVZAR, ZVZARARP and ZVZARZA. First, the difference between the two ZA implementations was highlighted. One of them assumes small roll and pitch angles and does not depend on the inertial sensor grade while the other depends on the sensor grade and not on the initial values of the roll and pitch. From an observability point of view, there is no difference in their observable subspaces. Since we consider stationary conditions, in most scenarios (but not in all of them) the actual roll and pitch angles are indeed small. Thus, we assumed small angles (zero mean with 3deg STD) and low grade sensors. A numerical comparison under those conditions showed that the ZA implementation assuming small error is preferred.

Next, the four measurement models were plugged in a regular EKF implementation. The results of all models matches the derived analytical observability analysis. The numerical comparison showed that ZVZARARP measurement model outperformed all other models. It obtained the lowest MC mean error results in all error-states. A field experiment conducted using a smartphone, held stationary, validated this conclusion.

Finally, to further improve the estimation performance four different adaptive filters, in the Kalman framework, were applied with the ZVZARARP measurement model. There, the EKF-R managed to improve the convergence rate of the gyroscopes biases with a cost of increased fluctuations in the roll and pitch error. A practical solution for such trade-off is to run in parallel two EKFs implementations, the regular one and EKF-R, and take the roll and pitch estimation results from the regular filter. If due to hardware or software capabilities this solution is not possible, then, if there is no limit on the time to complete the fine alignment process the regular EKF should be used. However, if there exists a time limit of several seconds (less than 10) EKF-R should be the implemented filter.

Although the paper focused on fine alignment applications, the measurement models as well as the analytical observability analysis, provided here, can be used also in other stationary condition scenarios such as land vehicles stopping at a red light or for any other reason, wheeled robots or other types of robots at rest and even a shoe-mounted INS for the periods when the shoe is on the ground.

REFERENCES

[1] D. Titterton and J. L. Weston, "Strapdown inertial navigation technology," in *The American Institute of Aeronautics and Astronautics and the Institution of Electrical Engineers*, 2nd ed. Stevenage, U.K.: Institution of Electrical Engineers, 2004.

[2] A. Noureldin, T. B. Karamat, and J. Georgy, *Fundamentals of Inertial Naviagtion, Satellite-Based Positioning and Their Integration*. New York, NY, USA: Springer, 2013.

[3] Y. F. Jiang, "Error analysis of analytic coarse alignment methods," *IEEE Trans. Aerosp. Electron. Syst.*, vol. 34, no. 1, pp. 334–337, Jan. 1998.

[4] F. O. Silva, E. M. Hemerly, and W. C. L. Filho, "Error analysis of analytical coarse alignment formulations for stationary SINS," *IEEE Trans. Aerosp. Electron. Syst.*, vol. 52, no. 4, pp. 1777–1796, Aug. 2016.

[5] E. Vaknin and I. Klein, "Coarse leveling of gyro-free INS," *Gyroscopy Navigat.*, vol. 7, no. 2, pp. 145–151, Apr. 2016.

[6] Y. Wu and X. Pan, "Velocity/position integration formula—Part I: Application to in-flight coarse alignment," *IEEE Trans. Aerosp. Electron. Syst.*, vol. 49, no. 2, pp. 1006–1023, Apr. 2013.

[7] X. Xu, Y. Sun, J. Gui, Y. Yao, and T. Zhang, "A fast robust in-motion alignment method for SINS with DVL aided," *IEEE Trans. Veh. Technol.*, vol. 69, no. 4, pp. 3816–3827, Apr. 2020.

[8] X. Xu, J. Gui, Y. Sun, Y. Yao, and T. Zhang, "A robust in-motion alignment method with inertial sensors and Doppler velocity log," *IEEE Trans. Instrum. Meas.*, vol. 70, pp. 1–13, 2021.

[9] I. Y. Bar-Itzhack and N. Berman, "Control theoretic approach to inertial navigation systems," *J. Guid., Control, Dyn.*, vol. 11, no. 3, pp. 237–245, May 1988.

[10] Y. F. Jiang and Y. P. Lin, "Error estimation of INS ground alignment through observability analysis," *IEEE Trans. Aerosp. Electron. Syst.*, vol. 28, no. 1, pp. 92–97, 1992.

[11] P. D. Groves, *Principles of GNSS, Inertial and Multisensor Integrated Navigation Systems*, 2nd ed. Norwood, MA, USA: Artech House, 2013.

[12] J. A. Farrell, *Aided Navigation GPS With High Rate Sensors*. New York, NY, USA: McGraw-Hill, 2008.

[13] A. Tsukerman and I. Klein, "Analytic evaluation of fine alignment for velocity aided INS," *IEEE Trans. Aerosp. Electron. Syst.*, vol. 54, no. 1, pp. 376–384, Feb. 2018.

[14] R. M. Rogers, *Applied Mathematics in Integrated Navigation Systems*. Reston, VA, USA: American Institute of Aeronautics and Astronautics, 2007.

[15] A. Ramanandan, A. Chen, and J. A. Farrell, "Observability analysis of an inertial navigation system with stationary updates," in *Proc. Amer. Control Conf.*, Jun. 2011, pp. 5292–5299.

[16] K. R. Britting, *Inertial Navigation Systems Analysis*. New York, NY, USA: Wiley-Interscience, 1971.

[17] F. O. Silva, E. M. Hemerly, and W. C. L. Filho, "On the measurement selection for stationary SINS alignment Kalman filters," *Measurement*, vol. 130, pp. 82–93, Dec. 2018.

[18] X. Xu, J. Lu, and T. Zhang, "A fast-initial alignment method with angular rate aiding based on robust Kalman filter," *IEEE Access*, vol. 7, pp. 51369–51378, 2019.

[19] J. Li, Y. Li, and B. Liuxs, "Fast fine initial self-alignment of INS in erecting process on stationary base," *J. Navigat.*, vol. 71, no. 3, pp. 697–710, May 2018.

[20] Y. Bar-Shalom, X. R. Li, and T. Kirubarajan, *Estimation With Applications to Tracking and Navigation: Theory Algorithms and Software*. Hoboken, NJ, USA: Wiley, 2004.

[21] J.-H. Wang and Y. Gao, "Land vehicle dynamics-aided inertial navigation," *IEEE Trans. Aerosp. Electron. Syst.*, vol. 46, no. 4, pp. 1638–1653, Oct. 2010.

[22] A. Brandt and J. F. Gardner, "Constrained navigation algorithms for strapdown inertial navigation systems with reduced set of sensors," in *Proc. Amer. Control Conf.*, vol. 3, Jun. 1998, pp. 1848–1852 vol.3.

[23] G. Dissanayake, S. Sukkarieh, E. Nebot, and H. Durrant-Whyte, "The aiding of a low-cost strapdown inertial measurement unit using vehicle model constraints for land vehicle applications," *IEEE Trans. Robot. Autom.*, vol. 17, no. 5, pp. 731–747, Oct. 2001.

[24] F. L. Lewis, L. Xie, and D. Popa, *Optimal and Robust Estimation*. Boca Raton, FL, USA: CRC Press, 2008.

[25] B. D. O. Anderson and J. B. Moore, *Optimal Filtering*. Englewood Cliffs, NJ, USA: Prentice-Hall, 1979.

[26] M. B. Rhudy and Y. Gu, "Online stochastic convergence analysis of the Kalman filter," *Int. J. Stochastic Anal.*, vol. 2013, 2013, Art. no. 240295.

[27] M. Rhudy, *Increasing the convergence rate of the Extended Kalman Filter*. New York, NY, USA: AIAA Aerospace, 2015.

[28] K. Reif and R. Unbehauen, "The extended Kalman filter as an exponential observer for nonlinear systems," *IEEE Trans. Signal Process.*, vol. 47, no. 8, pp. 2324–2328, Aug. 1999.
[29] U. Nusbaum and I. Klein, "Control theoretic approach to gyro-free inertial navigation systems," *IEEE Aerosp. Electron. Syst. Mag.*, vol. 32, no. 8, pp. 38–45, Aug. 2017.

ITZIK KLEIN (Senior Member, IEEE) received the B.Sc. and M.Sc. degrees in aerospace engineering and the Ph.D. degree in civil engineering from the Technion-Israel Institute of Technology, in 2004, 2007, and 2011, respectively. He is currently an Assistant Professor with the University of Haifa, where he is heading the Autonomous Navigation and Sensor Fusion Laboratory, Department of Marine Technologies. His research interests include navigation, novel inertial navigation architectures, autonomous underwater vehicles, sensor fusion, and estimation theory.

YAAKOV BAR-SHALOM (Life Fellow, IEEE) received the B.S. and M.S. degrees in electrical engineering from the Technion, in 1963 and 1967, respectively, and the Ph.D. degree in electrical engineering from Princeton University, in 1970. He is currently the Board of Trustees Distinguished Professor with the ECE Department and a Marianne E. Klewin Professor with the University of Connecticut. He is a member of the Connecticut Academy of Science and Engineering. He has been listed by academic.research.microsoft (top authors in engineering) as #1 among the researchers in aerospace engineering based on the citations of his work. He has published 600 articles and book chapters. He coauthored/edited eight books, including *Tracking and Data Fusion* (YBS Publishing, 2011). His current research interests include estimation theory, target tracking, and data fusion. He has been elected as a Fellow of IEEE for contributions to the theory of stochastic systems and of multitarget tracking. He was a co-recipient of the M. Barry Carlton Award for the best paper in the IEEE TAESystems, in 1995 and 2000. He received the J. Mignona Data Fusion Award from the DoD JDL Data Fusion Group, in 2002. He was awarded the IEEE Dennis J. Picard Medal for Radar Technologies and Applications, in 2008, and the Connecticut Medal of Technology, in 2012. He was a recipient of the 2015 ISIF Award for a Lifetime of Excellence in Information Fusion. This award has been renamed in 2016 as the Yaakov Bar-Shalom Award for a Lifetime of Excellence in Information Fusion. He was the General Chairman of the 1985 ACC, the General Chairman of FUSION 2000, the President of ISIF, in 2000 and 2002, and the Vice President for Publications, during 2004–2013. He served as an Associate Editor for the IEEE TRANSACTIONS ON AUTOMATIC CONTROL and *Automatica*. Since 1995, he has been a Distinguished Lecturer of the IEEE AESS.